ACS APPLIED MATERIALS & INTERFACES

Research Article

www.acsami.org

Novel Mn–Ce–Ti Mixed-Oxide Catalyst for the Selective Catalytic Reduction of NO_x with NH_3

Zhiming Liu,*[,†] Junzhi Zhu,[†] Junhua Li,[‡] Lingling Ma,[§] and Seong Ihl Woo[∥]

[†]State Key Laboratory of Chemical Resource Engineering, Beijing University of Chemical Technology, Beijing 100029, China

[‡]School of Environment, Tsinghua University, Beijing 100084, China

[§]Key Laboratory of Nuclear Radiation and Nuclear Energy Technology, Institute of High Energy Physics, Chinese Academy of Sciences, Beijing 100049, China

[∥]Department of Chemical and Biomolecular Engineering, Graduate School of EEWS(WCU), Korea Advanced Institute of Science and Technology, Daejeon 305-701, Republic of Korea

Supporting Information

ABSTRACT: Mn–Ce–Ti mixed-oxide catalyst prepared by the hydrothermal method was investigated for the selective catalytic reduction (SCR) of NO_x with NH_3 in the presence of oxygen. It was found that the environmentally benign Mn–Ce–Ti catalyst exhibited excellent NH_3-SCR activity and strong resistance against H_2O and SO_2 with a broad operation temperature window, which is very competitive for the practical application in controlling the NO_x emission from diesel engines. On the basis of the catalyst characterization, the dual redox cycles ($Mn^{4+} + Ce^{3+} \leftrightarrow Mn^{3+} + Ce^{4+}$, $Mn^{4+} + Ti^{3+} \leftrightarrow Mn^{3+} + Ti^{4+}$) and the amorphous structure play key roles for the high catalytic deNO_x performance. Diffuse reflectance infrared Fourier transform spectroscopy studies showed that the synergetic effect between Mn and Ce contributes to the formation of reactive intermediate species, thus promoting the NH_3-SCR to proceed.

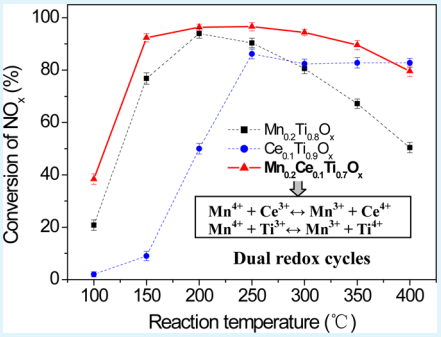

KEYWORDS: *nitrogen oxides, selective catalytic reduction, manganese–cerium–titanium mixed oxide, in situ drifts, redox cycle*

1. INTRODUCTION

NO_x removal from diesel engine exhaust remains one of the major challenges in environmental catalysis since the conventional three-way catalysts are no longer effective to reduce NO_x under lean-burn conditions.[1] Selective catalytic reduction (SCR) of NO_x with NH_3 (NH_3-SCR) is regarded as one of the most promising technologies for the abatement of NO_x from diesel engines.[1] Although V_2O_5–$WO_3(MoO_3)$/TiO_2 catalyst has been widely used in the NH_3-SCR for the removal of NO_x from stationary sources,[1,2] the practical application of this catalyst system has been restrained for diesel engines due to the inevitable problems including the toxicity of vanadium species and the poor low-temperature activity.[3] The temperature of the exhaust gas from diesel engine is mainly in the range of 150–350 °C.[4] Zeolite-based NH_3-SCR catalysts have been studied extensively for reducing NO_x from diesel engine in recent years. But they often exhibit insufficient activity at low temperatures.[3] To boost NO_x reduction at low temperatures for diesel engine, one method is placing a diesel oxidation catalyst (DOC) upstream of the SCR converter to convert a portion of NO to NO_2, thus promoting the fast SCR reaction.[5] However, the dynamic temperature and flow rate of the exhaust gases influence the oxidation activity of the DOC significantly; thus, the overall deNO_x efficiency over the SCR unit is limited. Therefore, it is desirable to develop environmentally benign NH_3-SCR catalysts, with high SCR performance in a wide temperature range, for the control of NO_x emitted from diesel engines.

Mn-containing catalysts, such as MnO_x/TiO_2 and MnO_x, exhibited relatively high activity for the low-temperature NH_3-SCR.[6,7] Amorphous manganese oxide was reported to be active for the NO_x reduction.[8] Cr–MnO_x mixed-oxide catalyst is highly active in the range of 120–220 °C, and the reduction of Mn^{4+} to Mn^{3+} plays an important role.[9] Thirupathi et al.[10] also reported that the high reducibility of MnO_2 phase was responsible for the high SCR activity of the nickel-doped Mn/TiO_2 catalyst.

Besides Mn-containing catalysts, Ce-based NH_3-SCR catalyst has also attracted attention due to the high oxygen storage capacity and excellent redox property of CeO_2.[11−13] For the Ce–Ti mixed-oxide catalyst, the amorphous CeO_2 was suggested to be favorable for the NH_3-SCR of NO_x.[14] The doping of tungsten to Ce/TiO_2 leads to an enhanced SCR activity due to the strong interaction between Ce and W.[15] MnO_x–CeO_2 mixed oxides showed high NH_3-SCR activity between 100 and 200 °C.[12,16] However, the narrow temperature window has restrained its application for the removal of NO_x from diesel engines.

Received: June 15, 2014
Accepted: July 21, 2014
Published: July 21, 2014

Considering that the redox property of the catalyst and the amorphous structure are closely related to the NH_3-SCR activity, the amorphous Mn−Ce−Ti mixed-oxide catalyst with dual redox cycles ($Mn^{4+} + Ce^{3+} \leftrightarrow Mn^{3+} + Ce^{4+}$, $Mn^{4+} + Ti^{3+} \leftrightarrow Mn^{3+} + Ti^{4+}$) was first fabricated, and it presented excellent NH_3-SCR activity and strong resistance against H_2O and SO_2 in a wide temperature window. The Mn−Ce−Ti catalyst could be a very competitive catalyst for the practical application in controlling the NO_x emission from diesel engines.

2. EXPERIMENTAL SECTION

2.1. Catalyst Preparation. The Mn−Ce−Ti catalysts with different ratios of Mn/Ce/Ti were prepared by the hydrothermal method. Appropriate amounts of $Mn(NO_3)_2{\cdot}3H_2O$, $Ce(NO_3)_3{\cdot}6H_2O$, and $Ti(SO_4)_2$ were dissolved in deionized water at room temperature and stirred for 1 h, then ammonia solution was added slowly to the above solution under vigorous stirring until pH is ca. 11. After stirring for 2 h, the obtained suspension was transferred to a Teflon-sealed autoclave and aged at 120 °C for 48 h. The obtained precipitate was filtered and washed with deionized water thoroughly. The resulting powder was dried at 120 °C for 12 h and then calcined in air at 500 °C for 6 h. For comparison, Mn−Ti and Ce−Ti catalysts were also prepared by the same preparation method as described above.

2.2. Catalytic Activity Measurement. The activity measurements were carried out in a fixed-bed quartz reactor using 0.12 g of catalyst of 40−60 mesh. The feed-gas mixture contained 500 ppm of NO, 500 ppm of NH_3, 0 or 5% H_2O, 0 or 50 ppm of SO_2, 5% O_2, and helium as the balance gas. The total flow rate of the feed gas was 300 cm^3 min^{-1}, corresponding to a gas hourly space velocity (GHSV) of 64 000 h^{-1}. The reaction temperature was increased from 100 to 400 °C in steps of 50 °C. The composition of the product gas was analyzed by a chemiluminescence NO/NO_2 analyzer (Thermal Scientific, model 42i-HL) and gas chromatograph (Shimadzu GC 2014 equipped with Porapak Q and Molecular sieve 5A columns). The activity data were collected when the catalytic reaction practically reached steady-state condition at each temperature. The effect of internal diffusion on the activity of the catalyst was investigated by comparing the catalytic activity over a variety of particle sizes of $Mn_{0.2}Ce_{0.1}Ti_{0.7}O_x$ catalyst including 50−70 and 60−80 mesh. The catalyst showed an essentially identical catalytic activity, regardless of the particle sizes of the catalyst. The reaction rate was obtained using the differential reactor over which the NO_x conversion was kept below 15%.

2.3. Catalyst Characterization. N_2 adsorption−desorption isotherms were obtained at liquid N_2 temperature (−196 °C) using a Quantachrome Nova Automated Gas Sorption System. The specific surface area was determined from the linear portion of the Brunauer−Emmett−Teller (BET) plot. The pore volume was calculated from the desorption branch of the N_2 adsorption isotherm using the Barrett−Joyner−Halenda (BJH) method. Prior to taking the surface area and pore volume measurement, the samples were degassed in a vacuum at 300 °C for 4 h. The elemental analysis of the prepared catalysts was performed by inductively coupled plasma atomic emission spectroscopy (ICP-AES) on a Plasma-Spec-I spectrometer.

X-ray diffraction (XRD) measurements were carried out on a Rigaku D/MAX-RB X-ray Diffractometer with Cu Kα radiation. The structure of catalyst was studied by the micro-Raman spectroscopy (Renisaw, InVia) under the 532 nm^{-1} excitation laser light. The morphologies of the catalysts were investigated by field-emission scanning electron microscopy (SEM) images obtained by a Zeiss Supra55 instrument operated at a beam energy of 20 kV. XPS measurements were conducted on an ESCALab220i-XL electron spectrometer from VG Scientific using 300 W Mg Kα radiation, calibrated internally by carbon deposit C 1s binding energy (BE) at 284.8 eV. A least-squares routine of peak fitting was used for the analysis of XPS spectra.

Temperature-programmed reduction (H_2-TPR) experiments were conducted on a chemisorption analyzer (Micromeritics, ChemiSorb 2720 TPx) under a 10% H_2 gas flow (50 mL min^{-1}) at a rate of 10 °C min^{-1} up to 650 °C.

2.4. In Situ DRIFTS Measurements. In situ DRIFTS experiments were performed on a Fourier transform infrared (FTIR) spectrometer (Nicolet 6700) equipped with a Harrick DRIFT cell containing ZnSe windows and MCT detector. Prior to each experiment, the sample was pretreated at 400 °C for 1 h in a flow of helium. The background spectrum was collected in flowing helium and was automatically subtracted from the sample spectrum. The reaction conditions were controlled as follows: 100 mL min^{-1} total flow rate, 500 ppm of NH_3 or 500 ppm of NO + 5% O_2, and helium balance. All spectra were recorded by accumulating 100 scans with a resolution of 4 cm^{-1}.

3. RESULTS AND DISCUSSION

3.1. Comparison of NH_3-SCR Performance . Figure 1 showed the NH_3-SCR performance of $Mn_{0.2}Ti_{0.8}O_x$, $Ce_{0.1}Ti_{0.9}O_x$, and $Mn_{0.2}Ce_{0.1}Ti_{0.7}O_x$ catalysts. It can be seen that $Ce_{0.1}Ti_{0.9}O_x$ exhibited low SCR activity below 250 °C, with only 10% NO_x conversion obtained at 150 °C. $Mn_{0.2}Ti_{0.8}O_x$ showed relatively high activity from 150 to 300 °C. The N_2 selectivity of $Mn_{0.2}Ti_{0.8}O_x$ and $Ce_{0.1}Ti_{0.9}O_x$ catalyst was noticeably decreased above 250 and 300 °C, respectively. And it was as low as about 40% at 400 °C. In contrast, $Mn_{0.2}Ce_{0.1}Ti_{0.7}O_x$ catalyst afforded highly remarkable catalytic activity. It demonstrated a wide operation temperature window with over 90% NO_x conversion obtained from 150 to 350 °C, and even at 150 °C, 92% of NO_x conversion can be achieved. The reaction rate of $Mn_{0.2}Ce_{0.1}Ti_{0.7}O_x$ at 150 °C was 12.2 μmol g^{-1} s^{-1}, which is much higher than that of $Mn_{0.2}Ti_{0.8}O_x$ (4.5 μmol g^{-1} s^{-1}) and $Ce_{0.1}Ti_{0.9}O_x$ (2.4 μmol g^{-1} s^{-1}) catalysts. More importantly, nearly 100% N_2 selectivity was obtained over $Mn_{0.2}Ce_{0.1}Ti_{0.7}O_x$ in the whole temperature range investigated.

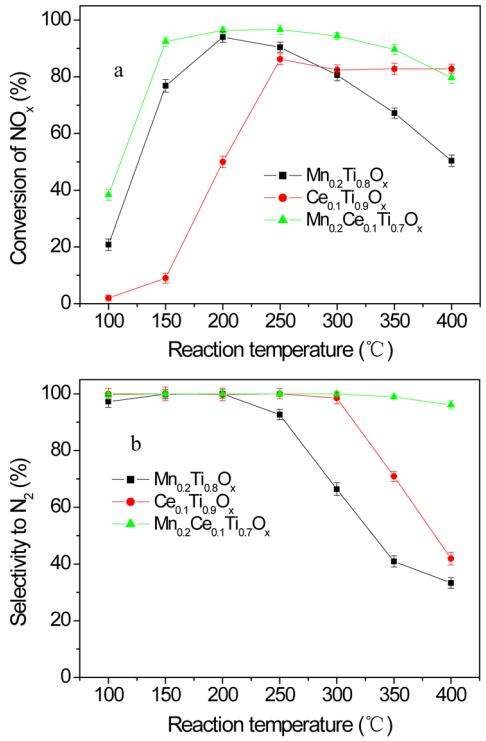

Figure 1. NH_3-SCR activity (a) and selectivity (b) of $Mn_{0.2}Ti_{0.8}O_x$, $Ce_{0.1}Ti_{0.9}O_x$, and $Mn_{0.2}Ce_{0.1}Ti_{0.7}O_x$ catalysts (500 ppm of NO, 500 ppm of NH_3, 5% O_2, balance He, GHSV = 64 000 h^{-1}).

dx.doi.org/10.1021/am5038164 | ACS Appl. Mater. Interfaces 2014, 6, 14500−14508

Therefore, $Mn_{0.2}Ce_{0.1}Ti_{0.7}O_x$ is very active and selective for the NH_3-SCR of NO_x.

Qi et al.[12] found that the molar ratios of Mn/(Mn + Ce) are closely related to the NH_3-SCR activity of MnO_x–CeO_2 mixed-oxide catalyst. Therefore, the activities of Mn–Ce–Ti catalysts with various ratios of Mn/Ce/Ti were also investigated, and the results are shown in Supporting Information, Figure S1. It can be seen that $Mn_{0.1}Ce_{0.1}Ti_{0.8}O_x$, $Mn_{0.1}Ce_{0.2}Ti_{0.7}O_x$, and $Mn_{0.3}Ce_{0.1}Ti_{0.6}O_x$ exhibited similar activity with wide activity temperature window. $Mn_{0.2}Ce_{0.1}Ti_{0.7}O_x$ exhibited a super low-temperature activity in the wide operating temperature window, indicating that it is promising for the control of NO_x emitted from diesel engine.

3.2. Effect of H_2O and SO_2. The effect of H_2O and SO_2 on the SCR activities of $Mn_{0.2}Ti_{0.8}O_x$, $Ce_{0.1}Ti_{0.9}O_x$, and $Mn_{0.2}Ce_{0.1}Ti_{0.7}O_x$ catalysts was also investigated. From the comparison of Figure 1 and Supporting Information, Figure S2, it can be seen that the presence of H_2O leads to the activity temperature window of $Mn_{0.2}Ce_{0.1}Ti_{0.7}O_x$ catalyst shifting to higher temperature by 50 °C. In the temperature range of 200–400 °C, more than 90% NO_x conversion was obtained, which is significantly higher than those obtained over $Mn_{0.2}Ti_{0.8}O_x$ and $Ce_{0.1}Ti_{0.9}O_x$ catalysts (see Supporting Information, Figure S2a). Even in the copresence of H_2O and SO_2, nearly 90% NO_x conversion was achieved from 200 to 400 °C. The conversion of NO_x is also much higher than those obtained over $Mn_{0.2}Ti_{0.8}O_x$ and $Ce_{0.1}Ti_{0.9}O_x$ catalysts (see Supporting Information, Figure S2b). The response of the NO_x conversion over $Mn_{0.2}Ce_{0.1}Ti_{0.7}O_x$ catalyst at 200 °C to the intermittent feed of H_2O and SO_2 was further investigated. As shown in Figure 2, the introduction of H_2O and SO_2 induced a slight

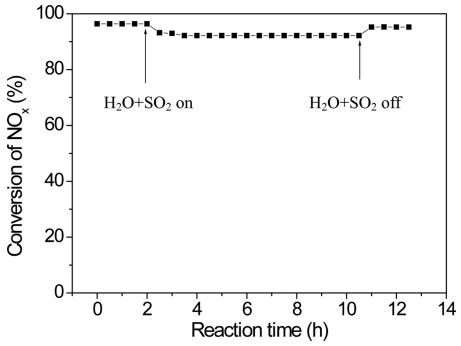

Figure 2. Response of the NO_x conversion over $Mn_{0.2}Ce_{0.1}Ti_{0.7}O_x$ catalyst at 200 °C to the intermittent feed of H_2O and SO_2 (500 ppm of NO, 500 ppm of NH_3, 5% O_2, 5% H_2O, 50 ppm of SO_2, balance He, GHSV = 64 000 h^{-1}).

decrease of the NO_x conversion. After excluding H_2O and SO_2 from the reactant feed, the NO_x conversion was almost recovered. Therefore, $Mn_{0.2}Ce_{0.1}Ti_{0.7}O_x$ catalyst displayed a satisfied resistance against H_2O and SO_2, which is very important for the potential deNO_x application.

3.3. BET Surface Area, XRD, Raman Spectra, and SEM. The chemical composition, BET surface area, and total pore volume of $Mn_{0.2}Ti_{0.8}O_x$, $Ce_{0.1}Ti_{0.9}O_x$, and $Mn_{0.2}Ce_{0.1}Ti_{0.7}O_x$ catalysts are listed in Table 1. The stoichiometry of the catalysts is close to the nominal values. It is evident that the surface area, pore diameter, and pore volume decreased in the order of $Mn_{0.2}Ce_{0.1}Ti_{0.7}O_x$ > $Ce_{0.1}Ti_{0.9}O_x$ > $Mn_{0.2}Ti_{0.8}O_x$. The high surface area of $Mn_{0.2}Ce_{0.1}Ti_{0.7}O_x$ could contribute to the high NH_3-SCR activity.

Figure 3 shows X-ray diffraction (XRD) patterns of $Mn_{0.2}Ti_{0.8}O_x$, $Ce_{0.1}Ti_{0.9}O_x$ and $Mn_{0.2}Ce_{0.1}Ti_{0.7}O_x$ catalysts.

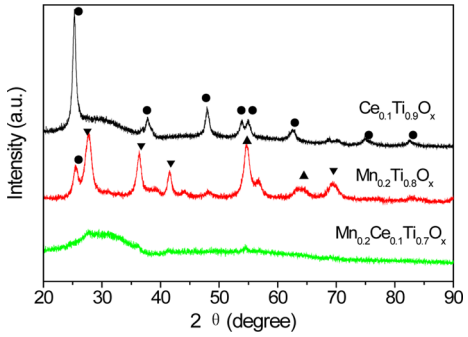

Figure 3. XRD patterns of $Mn_{0.2}Ti_{0.8}O_x$, $Ce_{0.1}Ti_{0.9}O_x$ and $Mn_{0.2}Ce_{0.1}Ti_{0.7}O_x$ catalysts: (●) anatase TiO_2; (▼) MnO_2; (▲) Mn_2O_3.

Over $Ce_{0.1}Ti_{0.9}O_x$ only an anatase structure (JCPDS 21–1272) was observed.[17] The peak ascribed to crystalline CeO_2 phase (JCPDS 34–0394) was absent, indicating that CeO_2 was highly dispersed on the surface of TiO_2. Besides the weak peak assigned to anatase phase, the peaks ascribed to MnO_2 (JCPDS 42–1169) and Mn_2O_3 (JCPDS 41–1442) appeared over $Mn_{0.2}Ti_{0.8}O_x$ catalyst.[8,18] No obvious peak was observed for $Mn_{0.2}Ce_{0.1}Ti_{0.7}O_x$, indicating a complete amorphous structure formed.[19] Raman spectroscopy experiment was conducted for further investigation of structure phases of these catalysts. Five bands, corresponding to the six Raman-active modes, namely, E_g (144, 197, and 639 cm^{-1}), A_{1g} (519 cm^{-1}), and B_{1g} (399 and 519 cm^{-1}), are observed over $Ce_{0.1}Ti_{0.9}O_x$ catalyst (see Figure 4). The Raman peak pattern is similar to the typical feature of anatase-structured TiO_2.[20] Since MnO_2 and Mn_2O_3 exhibited relatively weak Raman bands,[21] these phases were not detected by the present Raman spectra. Any peak ascribed to TiO_2, manganese, and cerium oxides are not detected over $Mn_{0.2}Ce_{0.1}Ti_{0.7}O_x$. This is in good accordance with the XRD result. These facts indicate that $Mn_{0.2}Ce_{0.1}Ti_{0.7}O_x$ mixed oxide is of amorphous structure, thereby maximizing the interaction among Mn, Ce, and Ti.[19] The strong interaction between TiO_2 support and the active metal oxides contributes to the NH_3-SCR activity.[22,23] The amorphous structure is usually of higher surface area than the crystallized one. Therefore, the BET surface area of Mn–Ce–Ti catalyst is as high as 217 m^2 g^{-1},

Table 1. Chemical Composition and Textual Properties of the Different Catalysts

catalyst	chemical composition[a]	surface area (m^2 g^{-1})	pore diameter (nm)	pore volume (cm^3 g^{-1})
$Mn_{0.2}Ti_{0.8}O_x$	$Mn_{0.19}Ti_{0.81}O_x$	101 ± 2.0	3.25 ± 0.08	0.19 ± 0.01
$Ce_{0.1}Ti_{0.9}O_x$	$Ce_{0.10}Ti_{0.90}O_x$	161 ± 4.2	3.27 ± 0.09	0.32 ± 0.01
$Mn_{0.2}Ce_{0.1}Ti_{0.7}O_x$	$Mn_{0.19}Ce_{0.10}Ti_{0.71}O_x$	217 ± 6.1	3.38 ± 0.10	0.48 ± 0.01

[a]Chemical composition determined by ICP-AES.

dx.doi.org/10.1021/am5038164 | ACS Appl. Mater. Interfaces 2014, 6, 14500–14508

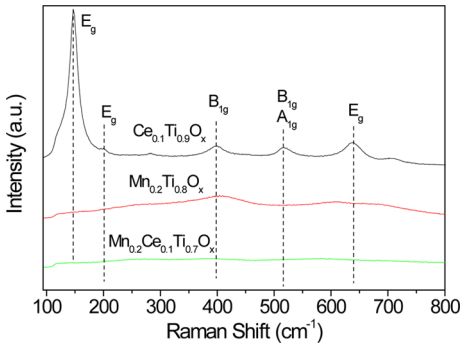

Figure 4. Raman spectra of $Mn_{0.2}Ti_{0.8}O_x$, $Ce_{0.1}Ti_{0.9}O_x$ and $Mn_{0.2}Ce_{0.1}Ti_{0.7}O_x$ catalysts.

which is much higher than that of TiO_2-based catalyst reported previously.[13,15] With varying the ratio of Mn and Ce, no obvious peak was observed on the Mn−Ce−Ti mixed-oxide catalysts (see Supporting Information, Figure S3), suggesting that the amorphous structure was still formed.[19]

The amorphous structure of Mn−Ce−Ti mixed oxide was also reflected from the SEM images. As illustrated in Figure 5, $Mn_{0.2}Ce_{0.1}Ti_{0.7}O_x$ is of amorphous structure, and some nanosheets interweave in the structure, which leads to the high surface area. $Mn_{0.2}Ti_{0.8}O_x$ is also mainly composed of amorphous structure. The crystallinity was increased for $Ce_{0.1}Ti_{0.9}O_x$ catalyst, over which small particles agglomerate, forming a structure like cauliflower.

3.4. H_2-TPR Analysis. Temperature-programmed reduction (H_2-TPR) analysis was conducted to investigate the reduction behavior of $Mn_{0.2}Ti_{0.8}O_x$, $Ce_{0.1}Ti_{0.9}O_x$, and $Mn_{0.2}Ce_{0.1}Ti_{0.7}O_x$ catalysts. As illustrated in Figure 6, two reduction peaks centered at ∼250 and ∼350 °C can be distinguished in the H_2-TPR profile of $Mn_{0.2}Ti_{0.8}O_x$ catalyst, which can be assigned to the reduction processes of $MnO_2 \rightarrow Mn_2O_3 \rightarrow MnO$.[24,25] $Ce_{0.1}Ti_{0.9}O_x$ exhibited two reduction peaks at ∼350 and 570 °C. The former small peak is probably assigned to the reduction of the surface oxygen of ceria, and the second reduction peak is due to the reduction of Ce^{4+} to Ce^{3+}.[26,27] Interestingly, the $Mn_{0.2}Ce_{0.1}Ti_{0.7}O_x$ catalyst possesses two overlapped reduction peaks centered at ∼350 and 486 °C, the former of which can be assigned to the two-step reduction process of MnO_2 via Mn_2O_3 to MnO, and the latter one is due to the reduction of Ce^{4+} to Ce^{3+}. Evidently, the reduction temperature of Ce^{4+} to Ce^{3+} was decreased, indicating that the ceria oxides becomes more reducible, which can be ascribed to the synergetic effect between Mn and Ce. The synergetic effect can effectively promote the redox properties of the Mn−Ce−Ti mixed-oxide catalyst.

3.5. XPS Analysis. To reveal the surface nature of the active sites over the catalyst systems X-ray photoelectron spectra (XPS) analysis was conducted. The XPS spectra of Mn 2p for $Mn_{0.2}Ti_{0.8}O_x$ and $Mn_{0.2}Ce_{0.1}Ti_{0.7}O_x$ catalysts are shown in Figure 7. For both catalysts two main peaks due to Mn $2p_{3/2}$ and $2p_{1/2}$ appear at ∼642.0 and 653.5 eV, respectively. To better understand the manganese oxide phases and their relative intensities, the peak-fitting deconvolution was performed on Mn $2p_{3/2}$ and $2p_{1/2}$ peaks. As shown in Figure 7, both Mn $2p_{3/2}$ and $2p_{1/2}$ spectra can be separated into two characteristic peaks: the peaks at 641.2 and 653.2 eV correspond to Mn^{3+}, and those at 642.7 and 654.1 eV correspond to Mn^{4+}.[28] The ratio of Mn^{3+}, calculated by $Mn^{3+}/(Mn^{3+} + Mn^{4+})$, over $Mn_{0.2}Ce_{0.1}Ti_{0.7}O_x$ (71.0%) was

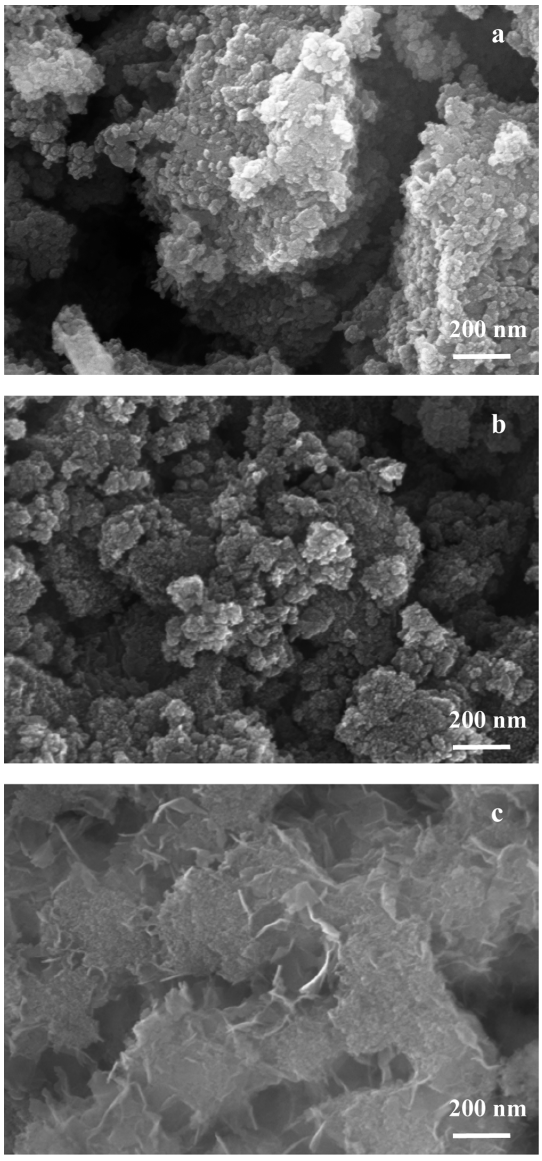

Figure 5. SEM images of $Mn_{0.2}Ti_{0.8}O_x$ (a), $Ce_{0.1}Ti_{0.9}O_x$ (b), and $Mn_{0.2}Ce_{0.1}Ti_{0.7}O_x$ (c) catalysts.

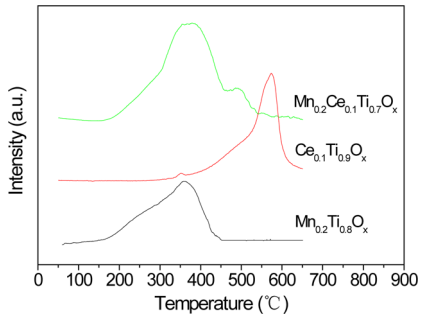

Figure 6. H_2-TPR profiles of $Mn_{0.2}Ti_{0.8}O_x$, $Ce_{0.1}Ti_{0.9}O_x$, and $Mn_{0.2}Ce_{0.1}Ti_{0.7}O_x$ catalysts.

significantly higher than that over $Mn_{0.2}Ti_{0.8}O_x$ (23.8%). The complex spectrum of Ce 3d was decomposed into eight components with the assignment defined in Figure 8. The subbands labeled u′ and v′ represent the $3d^{10}4f^1$ initial electronic state corresponding to Ce^{3+}, and those labeled u, u″, u‴, v, v″, and v‴ represent the $3d^{10}4f^0$ initial electronic state correspond-

dx.doi.org/10.1021/am5038164 | ACS Appl. Mater. Interfaces 2014, 6, 14500−14508

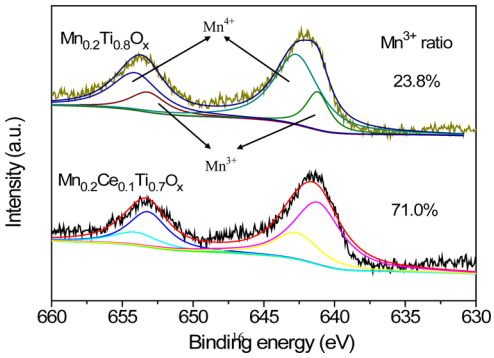

Figure 7. Mn 2p XPS spectra of $Mn_{0.2}Ti_{0.8}O_x$ and $Mn_{0.2}Ce_{0.1}Ti_{0.7}O_x$ catalysts.

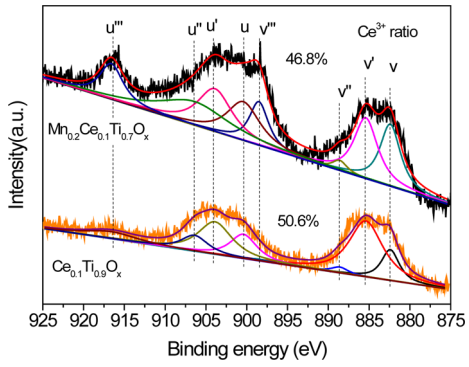

Figure 8. Ce 3d XPS spectra of $Ce_{0.1}Ti_{0.9}O_x$ and $Mn_{0.2}Ce_{0.1}Ti_{0.7}O_x$ catalysts.

ing to Ce^{4+}.[17] The high ratio of Ce^{3+} exists on both $Ce_{0.1}Ti_{0.9}O_x$ and $Mn_{0.2}Ce_{0.1}Ti_{0.7}O_x$ catalysts. The binding energy of Ti $2p_{3/2}$ for $Ce_{0.1}Ti_{0.9}O_x$ is 459.9 eV, which can be ascribed to Ti^{4+}(see Figure 9).[29] Compared with $Ce_{0.1}Ti_{0.9}O_x$ catalyst, the peak

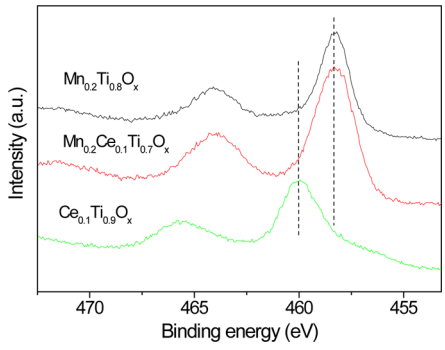

Figure 9. Ti 2p XPS spectra of $Mn_{0.2}Ti_{0.8}O_x$, $Ce_{0.1}Ti_{0.9}O_x$, and $Mn_{0.2}Ce_{0.1}Ti_{0.7}O_x$ catalysts.

position of Ti 2p for $Mn_{0.2}Ti_{0.8}O_x$ and $Mn_{0.2}Ce_{0.1}Ti_{0.7}O_x$ catalysts was shifted toward lower BE by 1.6 eV, suggesting that some Ti^{4+} could be reduced to Ti^{3+}.[30,31] The high reducibility of Ti contributes to improve the NH_3-SCR activity.[30] On the basis of the XPS results analysis, the high ratio of Mn^{3+} over $Mn_{0.2}Ce_{0.1}Ti_{0.7}O_x$ can be ascribed to the redox process of Ce^{4+}/Ce^{3+} and Ti^{4+}/Ti^{3+}, both of which could transfer electrons to Mn^{4+}.

3.6. In Situ DRIFTS Studies. *3.6.1. Adsorption of NO + O_2.* Figure 10a shows the DRIFT spectra of NO + O_2 on $Mn_{0.2}Ti_{0.8}O_x$ catalyst at different temperatures. The bands at

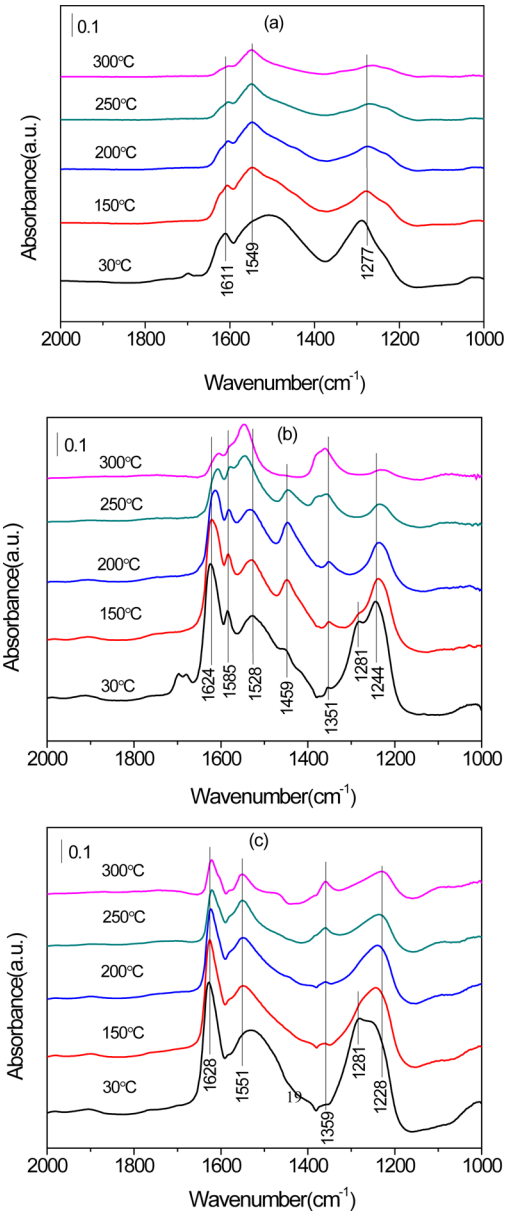

Figure 10. DRIFT spectra of NO + O_2 on $Mn_{0.2}Ti_{0.8}O_x$ (a), $Ce_{0.1}Ti_{0.9}O_x$ (b), and $Mn_{0.2}Ce_{0.1}Ti_{0.7}O_x$ (c) catalysts at different temperatures.

1611, 1549, and 1277 cm^{-1} can be assigned to the adsorbed NO_2 species,[12,32] monodentate nitrate,[33] and chelating nitrite,[34] respectively. As shown in Figure 10b, more NO_x adsorption bands were observed over $Ce_{0.1}Ti_{0.9}O_x$ catalyst. Besides the bands assigned to adsorbed NO_2 species (1624 cm^{-1})[12] and chelating nitrite (1281 cm^{-1}), those assigned to bidentate nitrate (1585 and 1528 cm^{-1}),[25] *trans*-$N_2O_2^{2-}$ (1459 cm^{-1}),[12] M−NO_2 nitro compounds (1351 cm^{-1}),[35] and bridging nitrate (1244 cm^{-1}),[25] respectively, were also observed. The DRIFT spectra of NO + O_2 on $Mn_{0.2}Ce_{0.1}Ti_{0.7}O_x$ catalyst at different temperatures was illustrated in Figure 10c. The intensity of the band ascribed to adsorbed NO_2 is high. Compared with Figure 10a,b, it is evident that the intensities of the bands assigned to monodentate nitrate and bridging nitrate over $Mn_{0.2}Ce_{0.1}Ti_{0.7}O_x$ catalyst are higher than those over $Mn_{0.2}Ti_{0.8}O_x$ and $Ce_{0.1}Ti_{0.9}O_x$, respectively. This fact suggests

dx.doi.org/10.1021/am5038164 | ACS Appl. Mater. Interfaces 2014, 6, 14500−14508

that the synergetic effect between Mn and Ce contributes to the formation of monodentate nitrate and bridging nitrate species.

3.6.2. Adsorption of NH_3. Figure 11 showed the DRIFT spectra of NH_3 adsorption on $Mn_{0.2}Ti_{0.8}O_x$, $Ce_{0.1}Ti_{0.9}O_x$, and

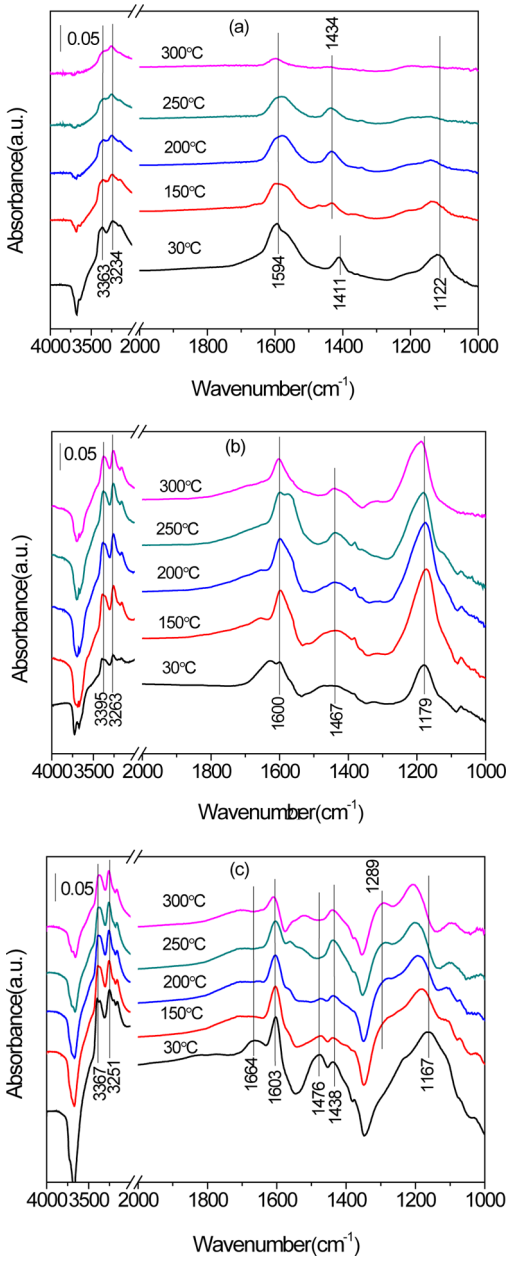

Figure 11. DRIFT spectra of NH_3 on $Mn_{0.2}Ti_{0.8}O_x$ (a), $Ce_{0.1}Ti_{0.9}O_x$ (b), and $Mn_{0.2}Ce_{0.1}Ti_{0.7}O_x$ (c) catalysts at different temperatures.

$Mn_{0.2}Ce_{0.1}Ti_{0.7}O_x$ catalysts at different temperatures. Several bands at 3363, 3234, 1594, 1411, and 1122 cm^{-1} were observed on $Mn_{0.2}Ti_{0.8}O_x$ catalyst (see Figure 11a). The bands at 1594 and 1122 cm^{-1} are related to the coordinated NH_3 bound to Lewis acid sites,[36,37] and those at 3363 and 3234 cm^{-1} can be ascribed to the N−H stretching vibration modes of the coordinated NH_3.[38] With increasing temperature, the peak at 1411 cm^{-1} was shifted to 1434 cm^{-1}, which is attributed to the NH_4^+ species on Brønsted acid sites.[6,39] On $Ce_{0.1}Ti_{0.9}O_x$ catalyst, the band ascribed to NH_4^+ species was absent, while the intensities of the bands assigned to the adsorbed NH_3 on Lewis acid sites are much higher than those observed on $Mn_{0.2}Ti_{0.8}O_x$ catalyst (see Figure 11b). As shown in Figure 11c, both the peaks ascribed to the adsorbed NH_3 on Lewis acid sites and NH_4^+ species on Brønsted acid sites (1664 and 1438 cm^{-1}) were observed on $Mn_{0.2}Ce_{0.1}Ti_{0.7}O_x$ catalyst, and their intensities were higher than those observed on $Mn_{0.2}Ti_{0.8}O_x$ catalyst. Moreover, the peak assigned to the deformation species of adsorbed NH_3 (1289 cm^{-1}) appeared.[40] This fact indicates that more NH_3 will be adsorbed and activated over $Mn_{0.2}Ce_{0.1}Ti_{0.7}O_x$ catalyst.

3.6.3. Reactivity of Surface-Adsorbed Species. Figure 12 presents the DRIFT spectra of $Mn_{0.2}Ce_{0.1}Ti_{0.7}O_x$ catalyst in a

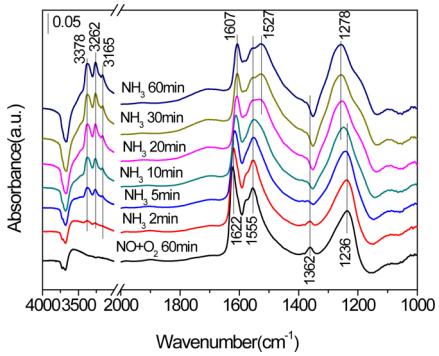

Figure 12. Dynamic changes of the in situ DRIFT spectra over $Mn_{0.2}Ce_{0.1}Ti_{0.7}O_x$ catalyst in a flow of NH_3 after the catalyst was pre-exposed to a flow of NO + O_2 for 60 min followed by helium purging for 30 min at 200 °C.

flow of NH_3 after the catalyst was pre-exposed to a flow of NO + O_2 for 60 min followed by helium purging for 30 min at 200 °C. It can be seen that switching the gas to NH_3 leads to the decrease of the intensities of NO_2 peak (1622 cm^{-1}), monodentate nitrate peak (1555 cm^{-1}), M−NO_2 nitro compounds and bridging nitrate peak (1236 cm^{-1}), indicating that these species are reactive in the NH_3-SCR process. Simultaneously, the peaks ascribed to the adsorbed NH_3 (3378, 3262, 3165, 1607, 1527, and 1278 cm^{-1}) appeared. Therefore, more reactive intermediates (NO_2, monodentate nitrate, M−NO_2 nitro compounds, and bridging nitrate) formed over $Mn_{0.2}Ce_{0.1}Ti_{0.7}O_x$ catalyst (see Figure 9c), thus leading to the high catalytic performance.

Figure 13 showed the DRIFT spectra of $Mn_{0.2}Ce_{0.1}Ti_{0.7}O_x$ catalyst in a flow of NO + O_2 after the catalyst was pre-exposed to a flow of NH_3 for 60 min followed by helium purging for 30 min at 200 °C. As illustrated in Figure 13, switching the gas to NO + O_2 leads to the decrease of the intensities of all bands assigned to ammonia species. And those bands vanished in 5 min. Meanwhile some new bands attributed to NO_x species appeared. This fact indicates that the adsorbed ammonia species are reactive in the NH_3-SCR of NO_x.

Zhang et al.[19] reported that amorphous CeO_2 phase was active for the SCR of NO_x by NH_3, while crystallized CeO_2 was deleterious to the activity. Kapteijn et al.[41] proposed that Mn_2O_3 exhibited high selectivity to N_2, while MnO_2 exhibited the highest activity. The presence of Mn^{3+} was also reported to play an important role in the SCR of NO_x by Li et al.[9] In the present study, the amorphous Mn−Ce−Ti mixed oxides were first fabricated by hydrothermal method, and they exhibited high NH_3-SCR activity in a wide temperature window. On the

dx.doi.org/10.1021/am5038164 | ACS Appl. Mater. Interfaces 2014, 6, 14500−14508

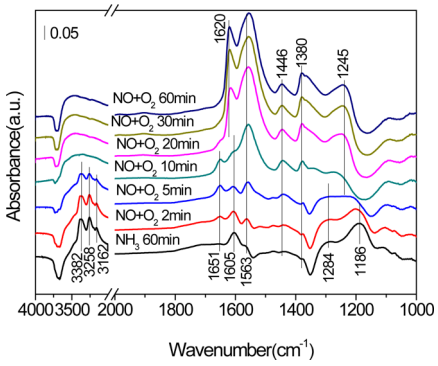

Figure 13. Dynamic changes of the in situ DRIFT spectra over $Mn_{0.2}Ce_{0.1}Ti_{0.7}O_x$ catalyst as a function of time in a flow of NO + O_2 after the catalyst was pre-exposed to a flow of NH_3 for 60 min followed by helium purging for 30 min at 200 °C.

basis of the catalyst characterization, it is a mixture of amorphous MnO_2, Mn_2O_3, CeO_2, Ce_2O_3, and TiO_2.

The redox properties are the key factors controlling the reactivity of NH_3-SCR catalysts.[11,17,22] For V_2O_5-based catalyst, the redox couples of V^{4+}/V^{5+} seemed to play an important role for the SCR reaction to proceed.[42] In the present study, the redox couples Mn^{4+}/Mn^{3+}, Ce^{4+}/Ce^{3+}, and Ti^{4+}/Ti^{3+} exist over Mn−Ce−Ti catalyst. Dual redox cycles ($Mn^{4+} + Ce^{3+} \leftrightarrow Mn^{3+} + Ce^{4+}$, $Mn^{4+} + Ti^{3+} \leftrightarrow Mn^{3+} + Ti^{4+}$) are available only for Mn−Ce−Ti catalyst and not for Mn−Ti and Ce−Ti catalysts, and both of the cycles can promote each other. This will result in a decrease in the energy required for the electron transfer between Mn, Ce, and Ti active sites. The electronic transfer is closely related to the activation of NO and NH_3 during the NH_3-SCR of NO_x.

The high ratio of Ce^{3+} and Ti^{3+} present over $Mn_{0.2}Ce_{0.1}Ti_{0.7}O_x$ catalyst can induce more oxygen vacancies to form,[13] which would promote the adsorption and activation of gas-phase oxygen. The activated oxygen atom plays an important role for the formation of NO_2.[32] From the comparison of Figure 10a,b, we can see that the intensities of the peaks ascribed to NO_2 and bridging nitrate over $Ce_{0.1}Ti_{0.9}O_x$ catalyst are higher than those observed over $Mn_{0.2}Ti_{0.8}O_x$ catalyst, indicating that the formation of NO_2 and bridging nitrate would be mainly over Ce active sites. Liu et al.[25] reported that the introduction of Mn to $FeTiO_x$ catalyst contributed to the formation of Brønsted acid sites on the catalyst surface. From Figure 11 we can see that the band ascribed to NH_4^+ species on Brønsted acid sites appeared over $Mn_{0.2}Ti_{0.8}O_x$ catalyst but not over $Ce_{0.1}Ti_{0.9}O_x$ catalyst. This fact suggests that Mn active sites would be responsible for the formation of NH_4^+. Therefore, we proposed the dual redox cycles for the activation of NO_x and NH_3 over Mn−Ce−Ti catalyst as depicted in Scheme 1. NO_2 could react with NH_4^+ to form NH_4NO_2 species, which reacted further to yield the NH_2NO. Then the NH_2NO decomposed to form N_2 and H_2O. Besides NO_2, the adsorbed monodentate nitrate and bridging nitrate would also react with the activated NH_4^+ or NH_3 following the Langmuir−Hinshelwood mechanism. On the other hand, the adsorbed NH_3 on Lewis acid sites would react with gas-phase NO (Eley−Rideal mechanism) to form N_2.

This research showed that the dual redox cycles ($Mn^{4+} + Ce^{3+} \leftrightarrow Mn^{3+} + Ce^{4+}$, $Mn^{4+} + Ti^{3+} \leftrightarrow Mn^{3+} + Ti^{4+}$) are the source of the synergistic effect on the catalytic properties of $Mn_{0.2}Ce_{0.1}Ti_{0.7}O_x$ catalyst, which facilitate the adsorption and activation of NO and NH_3, as shown in the in situ DRIFTS studies above, consequently leading to an improved NH_3-SCR performance.

Scheme 1. Dual Redox Cycles for the Activation of NO and NH_3

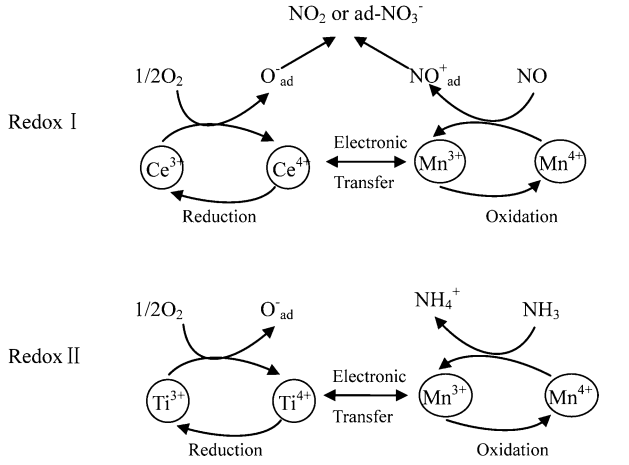

4. CONCLUSIONS

It has been demonstrated that an environmentally benign Mn−Ce−Ti mixed-oxide catalyst exhibited high catalytic activity for the NH_3-SCR of NO_x in a wide temperature range. Moreover, this catalyst displayed high resistance against H_2O and SO_2. The dual redox cycles ($Mn^{4+} + Ce^{3+} \leftrightarrow Mn^{3+} + Ce^{4+}$, $Mn^{4+} + Ti^{3+} \leftrightarrow Mn^{3+} + Ti^{4+}$) and the amorphous structure can account for the excellent NH_3-SCR catalytic performance of Mn−Ce−Ti catalyst. Compared with MnTi and CeTi catalysts, the adsorption and activation of NO and NH_3 was promoted over Mn−Ce−Ti catalyst, thus leading to an improvement of the NH_3-SCR performance. The present results have practical implications, as they may open new pathways for NO_x reduction at low temperatures, whereby diesel oxidation catalyst (DOC) positioned upstream of the SCR converter is no longer needed. Besides its application in diesel vehicles, this mixed-oxide catalyst is also promising for a number of modern stationary SCR applications.

■ ASSOCIATED CONTENT

Ⓢ Supporting Information

Figures showing catalyst activity versus temperature and XRD patterns. This material is available free of charge via the Internet at http://pubs.acs.org.

■ AUTHOR INFORMATION

Corresponding Author

*E-mail: liuzm@mail.buct.edu.cn. Phone: +86-10-64427356.

Notes

The authors declare no competing financial interest.

■ ACKNOWLEDGMENTS

This research was financially supported by the National Natural Science Foundation of China (21377010, 21325731), the Fundamental Research Funds for the Central Universities (YS1401), State Environmental Protection Key Laboratory of Sources and Control of Air Pollution Complex (SCAPC201402), and the Program for New Century Excellent

Talents of the Chinese Ministry of Education (NCET-13-0650).

REFERENCES

(1) Liu, Z. M.; Woo, S. I. Recent Advances in Catalytic DeNO$_x$ Science and Technology. *Catal. Rev.: Sci. Eng.* **2006**, *48*, 43−89.

(2) Busca, G.; Lietti, L.; Ramis, G.; Berti, F. Chemical and Mechanistic Aspects of the Selective Catalytic Reduction of NO$_x$ by Ammonia over Oxide Catalysts: A Review. *Appl. Catal., B* **1998**, *18*, 1−36.

(3) Long, R. Q.; Yang, R. T. Superior Fe-ZSM-5 Catalyst for Selective Catalytic Reduction of Nitric Oxide by Ammonia. *J. Am. Chem. Soc.* **1999**, *121*, 5595−5596.

(4) Clerc, J. C. Catalytic Diesel Exhaust Aftertreatment. *Appl. Catal., B* **1996**, *10*, 99−115.

(5) Forzatti, P.; Nova, I.; Tronconi, E. Enhanced NH$_3$ Selective Catalytic Reduction for NO$_x$ Abatement. *Angew. Chem., Int. Ed.* **2009**, *48*, 8366−8368.

(6) Smirniotis, P. G.; Peña, D. A.; Uphade, B. S. Low-Temperature Selective Catalytic Reduction (SCR) of NO with NH$_3$ by Using Mn, Cr, and Cu Oxides Supported on Hombikat TiO$_2$. *Angew. Chem., Int. Ed.* **2011**, *40*, 2479−2482.

(7) Kang, M.; Park, E. D.; Kim, J. M.; Yie, J. E. Manganese Oxide Catalysts for NO$_x$ Reduction with NH$_3$ at Low Temperatures. *Appl. Catal., A* **2001**, *327*, 261−269.

(8) Wu, Z. B.; Jiang, B. Q.; Liu, Y. Effect of Transition Metals Addition on the Catalyst of Manganese/Titania for Low-Temperature Selective Catalytic Reduction of Nitric Oxide with Ammonia. *Appl. Catal., B* **2008**, *79*, 347−355.

(9) Chen, Z.; Yang, Q.; Li, H.; Li, X.; Wang, L.; Tsang, S. C. Cr-MnO$_x$ Mixed-Oxide Catalysts for Selective Catalytic Reduction of NO$_x$ with NH$_3$ at Low Temperature. *J. Catal.* **2010**, *276*, 56−65.

(10) Thirupathi, B.; Smirniotis, P. G. Nickel-Doped Mn/TiO$_2$ as An Efficient Catalyst for the Low-Temperature SCR of NO with NH$_3$: Catalytic Evaluation and Characterizations. *J. Catal.* **2012**, *288*, 74−83.

(11) Qi, G.; Yang, R. T. A Superior Catalyst for Low-Temperature NO Reduction with NH$_3$. *Chem. Commun.* **2003**, *7*, 848−849.

(12) Qi, G.; Yang, R. T.; Chang, R. MnO$_x$-CeO$_2$ Mixed Oxides Prepared by Co-Precipitation for Selective Catalytic Reduction of NO with NH$_3$ at Low Temperatures. *Appl. Catal., B* **2004**, *51*, 93−106.

(13) Shan, W.; Liu, F.; He, H.; Shi, X.; Zhang, C. Novel Cerium-Tungsten Mixed-Oxide Catalyst for the Selective Catalytic Reduction of NO$_x$ with NH$_3$. *Chem. Commun.* **2011**, *47*, 8046−8048.

(14) Shan, W.; Liu, F.; He, H.; Shi, X.; Zhang, C. The Remarkable Improvement of a Ce−Ti-Based Catalyst for NO$_x$ Abatement, Prepared by a Homogeneous Precipitation Method. *ChemCatChem* **2011**, *3*, 1286−1289.

(15) Chen, L.; Li, J. H.; Ge, M. F.; Zhu, R. H. Enhanced Activity of Tungsten Modified CeO$_2$/TiO$_2$ for Selective Catalytic Reduction of NO$_x$ with Ammonia. *Catal. Today* **2010**, *153*, 77−83.

(16) Liu, Z. M.; Yi, Y.; Zhang, S. X.; Zhu, T. L.; Zhu, J. Z.; Wang, J. G. Selective Catalytic Reduction of NO$_x$ with NH$_3$ over Mn−Ce Mixed Oxide Catalyst at Low Temperatures. *Catal. Today* **2013**, *216*, 76−81.

(17) Shan, W.; Liu, F.; He, H.; Shi, X.; Zhang, C. A Superior Ce−W−Ti Mixed Oxide Catalyst for the Selective Catalytic Reduction of NO$_x$ with NH$_3$. *Appl. Catal., B* **2012**, *115/116*, 100−106.

(18) Chen, Z. H.; Wang, F. R.; Li, H.; Yang, Q.; Wang, L. F.; Li, X. H. Low-Temperature Selective Catalytic Reduction of NO$_x$ with NH$_3$ over Fe−Mn Mixed-Oxide Catalysts Containing Fe$_3$Mn$_3$O$_8$ Phase. *Ind. Eng. Chem. Res.* **2012**, *51*, 202−212.

(19) Li, P.; Xin, Y.; Li, Q.; Wang, Z.; Zhang, Z.; Zheng, L. Ce-Ti Amorphous Oxides for Selective Catalytic Reduction of NO with NH$_3$: Confirmation of Ce−O−Ti Active Sites. *Environ. Sci. Technol.* **2012**, *46*, 9600−9605.

(20) Yu, S.; Yun, H. J.; Lee, D. M.; Yi, J. Preparation and Characterization of Fe-Doped TiO$_2$ Nanoparticles as a Support for A High Performance CO Oxidation Catalyst. *J. Mater. Chem.* **2012**, *22*, 12629−12635.

(21) Hong, W.; Iwamoto, S.; Hosokawa, S.; Wada, K.; Kanai, H.; Inoue, M. Effect of Mn Content on Physical Properties of CeO$_x$-MnO$_y$ Support and BaO−CeO$_x$−MnO$_y$ Catalysts for Direct NO Decomposition. *J. Catal.* **2011**, *277*, 208−216.

(22) Li, Y.; Cheng, H.; Li, D.; Qin, Y.; Xie, Y.; Wang, S. WO$_3$/CeO$_2$−ZrO$_2$, A Promising Catalyst for Selective Catalytic Reduction (SCR) of NO$_x$ with NH$_3$ in Diesel Exhaust. *Chem. Commun.* **2008**, *12*, 1470−1472.

(23) Qi, G.; Yang, R. T.; Chang, R. Low-Temperature Selective Catalytic Reduction of NO with NH$_3$ over Iron and Manganese Oxides Supported on Titania. *Appl. Catal., B* **2003**, *44*, 217−225.

(24) Chen, H.; Sayari, A.; Adnot, A.; Larachi, F. Composition−Activity Effects of Mn−Ce−O Composites on Phenol Catalytic Wet Oxidation. *Appl. Catal., B* **2001**, *32*, 195−204.

(25) Liu, F. D.; He, H.; Ding, Y.; Zhang, C. B. Effect of Manganese Substitution on the Structure and Activity of Iron Titanate Catalyst for the Selective Catalytic Reduction of NO with NH$_3$. *Appl. Catal., B* **2009**, *93*, 194−204.

(26) Thirupathi, B.; Smirniotis, P. G. Co-Doping a Metal (Cr, Fe, Co, Ni, Cu, Zn, Ce, and Zr) on Mn/TiO$_2$ Catalyst and Its Effect on the Selective Reduction of NO with NH$_3$ at Low Temperatures. *Appl. Catal., B* **2011**, *110*, 195−206.

(27) Yang, D.; Wang, L.; Sun, Y.; Zhou, K. Synthesis of One-Dimensional $Ce_{1-x}Y_xO_{2-x/2}$ ($0 \le x \le 1$) Solid Solutions and Their Catalytic Properties: The Role of Oxygen Vacancies. *J. Phys. Chem. C* **2010**, *114*, 8926−8932.

(28) Kang, M.; Park, E. D.; Kim, J. M.; Yie, J. E. Manganese Oxide Catalysts for NO$_x$ Reduction with NH$_3$ at Low Temperatures. *Appl. Catal., A* **2007**, *327*, 261−269.

(29) Oku, M.; Wagatsuma, K.; Kohikib, S. Ti 2p and Ti 3p X-ray Photoelectron Spectra for TiO$_2$, SrTiO$_3$, and BaTiO$_3$. *Phys. Chem. Chem. Phys.* **1999**, *1*, 5327−5331.

(30) Seo, P. W.; Cho, S. P.; Hong, S. H.; Hong, S. C. The Influence of Lattice Oxygen in Titania on Selective Catalytic Reduction in the Low-Temperature Region. *Appl. Catal., A* **2010**, *380*, 21−27.

(31) Lee, J. Y.; Hong, S. H.; Cho, S. P.; Hong, S. C. The Study of DeNO$_x$ Catalyst in Low Temperature Using Nano-Sized Supports. *Curr. Appl. Phys.* **2006**, *6*, 996−1001.

(32) Chen, L.; Li, J. H.; Ge, M. F. DRIFT Study on Cerium-tungsten/Titiania Catalyst for Selective Catalytic Reduction of NO$_x$ with NH$_3$. *Environ. Sci. Technol.* **2010**, *44*, 9590−9596.

(33) Liu, Z.; Woo, S. I.; Lee, W. S. In situ FT-IR Studies on the Mechanism of Selective Catalytic Reduction of NO$_x$ by Propene over SnO$_2$/Al$_2$O$_3$ Catalyst. *J. Phys. Chem. B* **2006**, *110*, 26019−26023.

(34) Costa, C. N.; Efstathiou, A. M. Transient Isotopic Kinetic Study of the NO/H$_2$/O$_2$(Lean de-NO$_x$) Reaction on Pt/SiO$_2$ and Pt/La-Ce-Mn-O Catalysts. *J. Phys. Chem. B* **2004**, *108*, 2620−2630.

(35) Wu, Z. B.; Jiang, B. Q.; Liu, Y.; Wang, H. Q.; Jin, R. B. DRIFT Study of Manganese/Titania-Based Catalysts for Low-Temperature Selective Catalytic Reduction of NO with NH$_3$. *Environ. Sci. Technol.* **2007**, *41*, 5812−5817.

(36) Lietti, L.; Nova, I.; Ramis, G.; DallÏAcqua, L.; Busca, G.; Giamello, E.; Forzatti, P.; Bregani, F. Characterization and Reactivity of V$_2$O$_5$-MoO$_3$/TiO$_2$ De-NO$_x$ SCR Catalysts. *J. Catal.* **1999**, *187*, 419−435.

(37) Larrubia, M. A.; Ramis, G.; Busca, G. An FT-IR Study of the Adsorption of Urea and Ammonia over V$_2$O$_5$-MoO$_3$-TiO$_2$ SCR Catalysts. *Appl. Catal., B* **2000**, *27*, L145−L151.

(38) Dall'Acqua, L.; Nova, I.; Lietti, L.; Ramis, G.; Busca, G.; Giamello, E. Spectroscopic Characterization of MoO$_3$/TiO$_2$ DeNO$_x$-SCR Catalysts: Redox and Coordination Properties. *Phys. Chem. Chem. Phys.* **2000**, *2*, 4991−4998.

(39) Lin, S. D.; Gluhoi, A. C.; Nieuwenhuys, B. E. Ammonia Oxidation over Au/MO$_x$/c-Al$_2$O$_3$-Activity, Selectivity, and FTIR Measurements. *Catal. Today* **2004**, *90*, 3−14.

(40) Yang, S.; Wang, C.; Li, J.; Yan, N.; Ma, L.; Chang, H. Low-Temperature Selective Catalytic Reduction of NO with NH$_3$ over Mn−Fe Spinel: Performance, Mechanism and Kinetic Study. *Appl. Catal., B* **2011**, *110*, 71−80.

(41) Kapteijn, F.; Singoredjo, L.; Andreini, A.; Moulijn, J. A. Activity and Selectivity of Pure Manganese Oxides in the Selective Catalytic Reduction of Nitric Oxide with Ammonia. *Appl. Catal., B* **1994**, *3*, 173−189.
(42) Topsøe, N. Y.; Dumesic, J. A.; Topsøe, H. Vanadia/Titania Catalysts for Selective Catalytic Reduction (SCR) of Nitric Oxide by Ammonia. II: Studies of Active Sites and Formulation of Catalytic Cycles. *J. Catal.* **1995**, *151*, 241−252.